Uniform CaWO$_4$:Ln (Ln = Eu^{3+}, Dy^{3+}) phosphors: solvothermal synthesis and luminescent properties

W. WANG[a], W. PAN[b], Y. DAI[a], S. GAI[a], P. YANG[a,*]
[a] *College of Material Science and Chemical Engineering, Harbin Engineering University, Harbin 150001, P. R. China*
[b] *College of Chemical Engineering and Food, Zhongzhou University , Zhengzhou 450044, China*

Uniform CaWO$_4$:Ln (Ln = Eu^{3+}, Dy^{3+}) phosphors were successfully synthesized via the micro-emulsion mediated solvothermal process. The as-synthesized samples were well characterized by XRD, FESEM, TEM, XPS, photoluminescence (PL) spectra, and the kinetic decays, respectively. It is found that the as-synthesized phosphors are of high crystallinity and purity with regular octahedral morphology. Upon excitation by ultraviolet radiation, the CaWO$_4$:Eu^{3+} phosphors show the characteristic $^5D_0$–$^7F_{1-4}$ emission lines of Eu^{3+}, while the CaWO$_4$:Dy^{3+} exhibits the characteristic $^4F_{9/2}$–$^6H_{13/2-15/2}$ emission lines of Dy^{3+}. It should be noted the PL intensities of the phosphors can be tuned by altering the doping concentration of Eu^{3+} and Dy^{3+}.

1. Introduction

During the past decade, tungstate composites have attracted much interest due to their special interesting properties, such as high chemical stability, high average refractive index, high X-ray absorption coefficient, high light yield, short decay time, and low afterglow as a self-activating phosphor [1], which show potential applications in the fields of photoluminescence [2], catalysis [3], optical fibers [4], and magnetic materials [5]. Recently, rare earth (RE) ions doped phosphors are of special attention because the corresponding bulk materials have practical applications in lighting and display [6–10]. Additionally, some rare earth ions such as Eu^{3+} and Dy^{3+} activated tungstates can be considered as a very promising luminescent material due to their high energy transfer efficiency. Up to now, a large number of rare earth doped tungstates phosphors have been fabricated and investigated by various techniques including Czochralski method [11], co-precipitation method [12], high-temperature solid state reaction [13], spray pyrolysis route [14], and so on. Among the various synthetic techniques, hydrothermal process may produce a highly crystalline product without further post-calcination, which performed at a mild reaction conditions (reaction temperature < 250 °C). Moreover, the hydrothermal method has proved to be a more effective way than the conventional solid-state reaction to dope Eu^{3+} ions for energy transfer from WO$_4^{2-}$ groups to Eu^{3+} ions [15]. Therefore, the solvothermal micro-emulsion route should provide a unique approach for the synthesis of tungstates phosphors with high crystallinity and special morphology.

So far, the work on the solvothermal synthesis of rare earth ions (Eu^{3+}, Dy^{3+}) doped CaWO$_4$ through a micro-emulsion process has been rarely reported. Herein, we proposed the synthesis of Eu^{3+}/Dy^{3+} doped CaWO$_4$ micro-structured phosphors with uniform morphology via a facile CTAB/water/*n*-octane/*n*-butonal micro-emulsion process based on the solvothermal crystallinization. The structure, morphology, and luminescent properties of the as-prepared phosphors were characterized by means of XRD, FESEM, TEM, XPS, and optical spectra, respectively. The kinetic decay time of the samples was also examined as well.

2. Experimental details

All the chemicals used in the experiment were of analytical grade and used without further purification. The doping concentration of Eu^{3+} was 5 mol% to Ca^{2+} in the CaWO$_4$:Eu^{3+} phosphor. Typically, 0.017 g of Eu(NO$_3$)$_3$, 0.224 g of Ca(NO$_3$)$_2$·4H$_2$O and 4 g of CTAB were dissolved in the mixed solvent containing 2 mL of H$_2$O, 3.95 mL of *n*-butanol and 15.43 mL of *n*-octane. Then the reverses micelle I was obtained. The reverses micelles II was prepared by dissolving 0.246 g of (NH$_4$)$_6$H$_2$W$_{12}$O$_{40}$ in the same microemulsion solvent. Subsequently, the two reverses micelles solutions were mixed rapidly with intense stirring. After stirred intensely for 30 min, the resulting solution was transferred into a 50 mL sealed Teflon autoclave and heated at 200 °C for 24 h. The final products were separated from the reverses micelles solution by centrifugation. The obtained precipitate was washed five times with a mixed solution of methanol and dichloromethane (volume ratio = 1:1), followed by centrifugal recovery and drying in vacuum at 60 °C for 12 h. In this way, the Eu^{3+} doped calcium tungstate was obtained, which was designated as CaWO$_4$:Eu^{3+}. Dy^{3+} doped CaWO$_4$ with the doping concentration of 3 mol% was prepared through the same process.

Powder X-ray diffraction (XRD) patterns were obtained on a Rigaku TR III diffractometer using Cu Kα radiation (λ = 0.15405 nm). Field emission scanning electron microscope (FESEM) study was performed on a XL30 microscope (Philips) equipped with an energy-dispersive X-ray spectrum (EDS, JEOL JXA-840). Transmission electron microscope (TEM) and high-resolution transmission electron microscope (HRTEM) images were recorded on a FEI Tecnai G^2 S-Twin with an acceleration voltage of 200 kV. The X-ray photoelectron spectra (XPS) were taken on a VG ESCALAB MK II electron energy spectrometer using Mg Kα (1253.6 eV) as the X-ray excitation source. The exact doping concentrations of Eu^{3+} in the resulting materials were determined by Inductively Coupled Plasma (ICP) performed on an ICP–PLASMA 1000 apparatus. The UV–vis excitation and emission spectra were obtained on a Hitachi F-4500 spectrofluorimeter equipped with a 150 W xenon lamp as the excitation source. Luminescence decay curves were obtained from a Lecroy Wave Runner 6100 Digital Oscilloscope (1 GHz) using a 250 nm laser (pulse width = 4 ns, gate = 50 ns) as the excitation source (Continuum Sunlite OPO).

3. Results and discussion

3.1. Structure characterization

The crystallinity and phase purity of the CaWO$_4$:Eu^{3+} and CaWO$_4$:Dy^{3+} crystals were examined by XRD, as shown in Fig. 1, and the standard data for the tetragonal CaWO$_4$ are also presented for comparison. It can be seen that the CaWO$_4$:Ln (Ln = Eu^{3+}, Dy^{3+}) phosphors show sharp diffraction peaks, revealing the high crystallinity of the samples. In addition, all the diffraction peaks can be well indexed to a tetragonal CaWO$_4$ in $I41/$a space group (JCPDS No. 41–1431). No other phases associated with doped component can be detected, suggesting the high purity of the two samples and the rare-earth ions have been uniformly incorporated into the host lattice of CaWO$_4$. Furthermore, the calculated lattice constants of a = b = 0.5225 nm, c = 1.1345 nm for CaWO$_4$:Eu^{3+} and a = b = 0.5233 nm, c = 1.1352 nm for CaWO$_4$:Dy^{3+} are well consistent with the standard data of a = b = 0.5243 nm, c = 1.1373 nm (JCPDS 41–1431). Furthermore, the respective doping concentration of Eu^{3+} in CaWO$_4$:Eu^{3+} and Dy^{3+} in CaWO$_4$:Dy^{3+} are determined to be 2.51 wt.% and 1.61 wt.% by ICP analysis, which are much close to the stoichiometric values (2.59 wt.% or 5 mol% to Ca^{2+} in CaWO$_4$:Eu^{3+} and 1.67 wt.% or 3 mol% to Ca^{2+} in CaWO$_4$:Dy^{3+}).
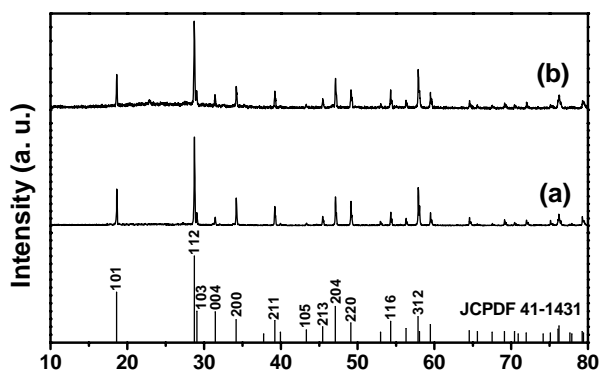
Fig. 1. XRD patterns of pure CaWO$_4$:Eu^{3+} (a), CaWO$_4$:Dy^{3+} (b), and the standard data for CaWO$_4$ (JCPDS 41–1431).

3.2. Morphology

The morphologies of the samples were well examined by the SEM and TEM techniques. Fig. 2 shows the SEM image, EDS, TEM image, and the corresponding HRTEM image of the CaWO$_4$:Eu^{3+} phosphors, respectively. The SEM image (Fig. 2a) reveals that the product is composed of exclusively octahedral crystals with a relatively uniform size, indicating the high yield of the product obtained by this facile solvothermal method. In particular, the high-magnification SEM image (Fig. 1a, inset) exhibits a perfect octahedral single crystal of the as-synthesized sample. The analysis of the single crystal shows that the crystal has average length of 5 μm for one border of the octahedral. The formation process of the octahedral morphology can be explained as following. It is well accepted that single-crystal particles usually have specific shapes which are caused by the enclosing of the crystallographic facets with lower energy [16,17]. In the case of CaWO$_4$:Eu^{3+}, octahedra are enclosed by (101) planes which have the lowest surface energy for the tetragonal crystal structure, resulting in the formation of the octahedral crystals. The signals of calcium (Ca), tungsten (W), oxygen (O), and europium (Eu) in the EDS (Fig. 2b) of CaWO$_4$:Eu^{3+} indicates the corresponding element in the product (the C signal is from the carbon substrate for measurement). The detained microstructure of the CaWO$_4$:Eu^{3+} has been further examined by TEM measurement. Fig. 2c exhibits the hexagonal projection of the single octahedral crystal, which is in good agreement with the SEM result. The lattice fringes in the HRTEM image (Fig. 2d) are clearly observed, confirming the high crystallinity of as-synthesized CaWO$_4$:Eu^{3+} phosphor. The lattice fringes of (112) planes with an interplanar distance of 0.31 nm are marked by the arrow. The calculated interplanar distance agrees well with the d112 spacing of the literature value (0.3105 nm) (JCPDS 41–1431).
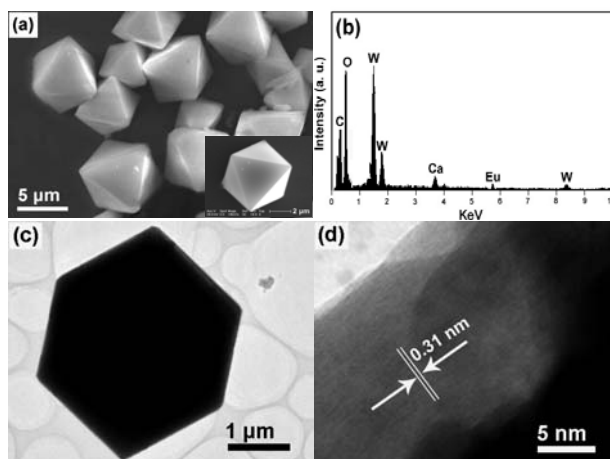
Fig. 2. SEM image (a), EDS (b), TEM image (c), and HRTEM image (d) of the as-synthesized $CaWO_4:Eu^{3+}$.

XPS technique has been proven a useful tool for qualitatively determining the surface component and composition of a material. XPS of the $CaWO_4:Eu^{3+}$ product is depicted in Fig. 3. The spectra show the binding energy of Eu (3d5/2, 1132.5 eV), Ca (2p, 347.8 eV), O (1s, 532.5 eV), and W (4f5/2, 34.8 eV; 4f3/2, 36.9 eV; 4p, 427 eV), respectively. By combination of the XRD results, it can be deduced that these signals can be assigned to the $CaWO_4:Eu^{3+}$ phosphor.

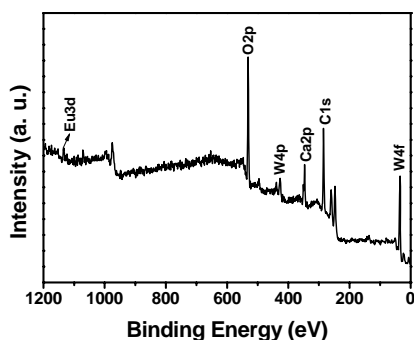Fig. 3. XPS of the as-synthesized $CaWO_4:Eu^{3+}$.

3.3. Photoluminescence (PL) properties

The PL properties of the samples were characterized by the PL excitation and emission spectra, as shown in Fig. 4. In the excitation spectrum monitored by the Eu^{3+} $^5D_0 \rightarrow ^7F_2$ transition at 612 nm for $CaWO_4:Eu^{3+}$ (Fig. 4a, left), the broad band at 248 nm can be due to the WO_4^{2-} groups. Several sharp peaks assigned to $^7F_0 \rightarrow ^5H_6$ (323 nm), $^7F_0 \rightarrow ^5D_4$ (366 nm), $^7F_0 \rightarrow ^5G_2$ (386 nm), $^7F_0 \rightarrow ^5L_6$ (396 nm), $^7F_0 \rightarrow ^5D_3$ (418 nm), $^7F_0 \rightarrow ^5D_2$ (469 nm) are clearly observed [18]. Upon excitation into the WO_4^{2-} groups at 248 nm, the characteristic emission of Eu^{3+} from the excited $^5D_0$ level is apparent in the emission spectrum (Fig. 4a, right). The locations of the emission lines together with their assignments are labeled in the figure. It can be seen that the emission of Eu^{3+} is dominated by the red $^5D_0 \rightarrow ^7F_2$ hypersensitive transition. The excitation and emission spectra of the $CaWO_4.Dy^{3+}$ are shown in Fig. 4b. Similar to that in $CaWO_4:Eu^{3+}$, a strong band at 231 nm attributed to the WO_4^{2-} group can be observed. Excitation into the WO_4^{2-} group at 231 nm yields the characteristic emission of Dy^{3+} at 479 nm, 487 nm ($^4F_{9/2} \rightarrow ^6H_{15/2}$) and 573 nm ($^4F_{9/2} \rightarrow ^6H_{13/2}$), which indicates that an efficient energy transfer also occurs from WO_4^{2-} to Dy^{3+}.

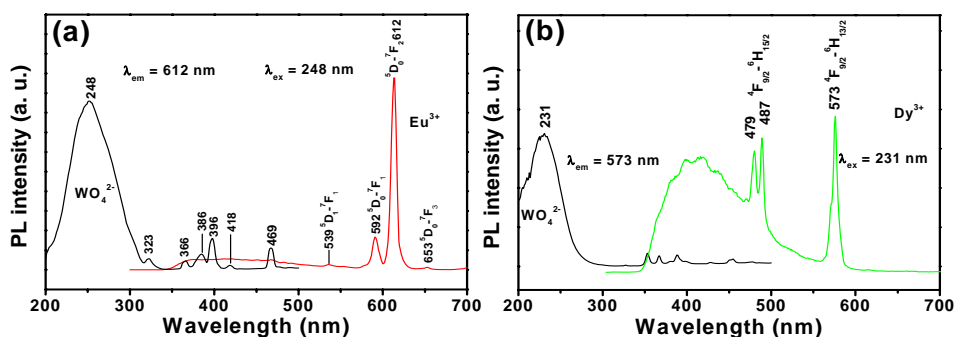Fig. 4. Excitation (left) and emission (right) spectra of the $CaWO_4:Eu^{3+}$ (a) and $CaWO_4:Dy^{3+}$ (b) phosphors.

The decay curves for Eu^{3+} in $CaWO_4:Eu^{3+}$ and Dy^{3+} in $CaWO_4:Dy^{3+}$ are shown in Fig. 5, respectively. It can be seen that the curves can be well fitted into a double-exponential function as $I = A_1\exp(-t/\tau_1) + A_2\exp(-t/\tau_2)$ (τ_1 and τ_2 are the fast and slow components of the luminescence lifetimes, A_1 and A_2 are the fitting parameters). The calculated average lifetime for $^5D_0\rightarrow^7F_2$ (612 nm) of Eu^{3+} and $^4F_{9/2}\rightarrow^6H_{13/2}$ (573 nm) of Dy^{3+} are 1.29 ms and 0.21 ms determined by the formula as $\tau = (A_1\tau_1^2 + A_2\tau_2^2) / (A_1\tau_1 + A_2\tau_2)$ [19].
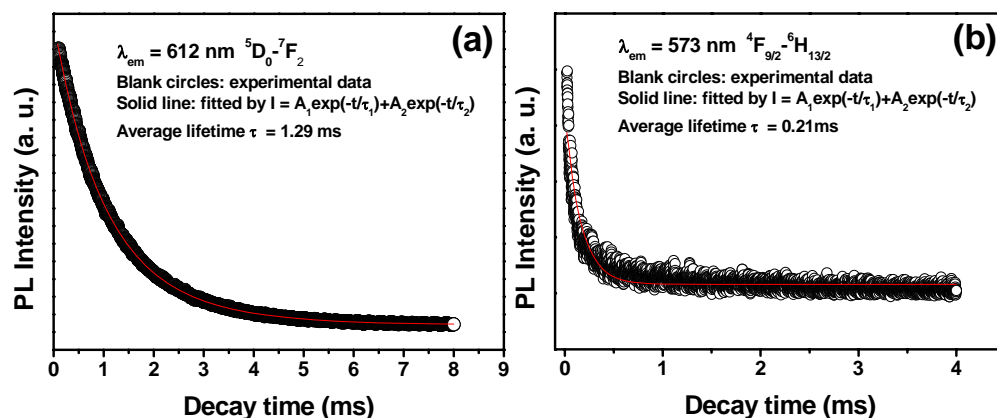

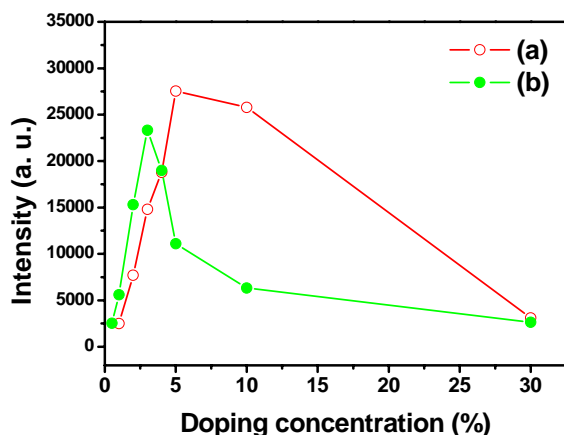Fig. 5. Decay curves of the $CaWO_4:Eu^{3+}$ (a) and $CaWO_4:Dy^{3+}$ (b) phosphors.

Fig. 6. The PL emission intensity of Eu^{3+} in $CaWO_4:Eu^{3+}$ (a) and Dy^{3+} in $CaWO_4:Dy^{3+}$ (b) as a function of the doping concentration.

3.4. Tuning of photoluminescence (PL) intensities

Effect of the doping concentration on the PL emission intensities of doped rare earth ions is investigated, which is shown in Fig. 6. It can be seen that the PL emission intensities increase with the doping concentration of Eu^{3+}, reaching a maximum at 5 mol% to Ca^{2+}, then decrease with further increased concentration due to the enhanced concentration quenching effect. Similar to that of Eu^{3+}, the doping concentration of Dy^{3+} has been optimized to 3 mol% for achieving the highest PL intensity for $CaWO_4:Dy^{3+}$ (Fig. 6b). The results reveal that the PL intensities of the sample can be tuned by altering the synthesis conditions.

4. Conclusions

In summary, luminescent Eu^{3+}/Dy^{3+} doped $CaWO_4$ crystals has been synthesized via a simple hydrothermal micro-emulsion process. The as-synthesized phosphors exhibit regular octahedral morphology with relatively narrow size distribution. The obtained $CaWO_4:Ln$ (Ln = Eu^{3+}, Dy^{3+}) phosphors show the respective characteristic emission lines of Eu^{3+} and Dy^{3+} upon UV excitation. The decay curve well fits into a double exponential function. Moreover, the PL intensities can be tuned by altering the concentration of the doped rare earth ions. The doping concentrations of Eu^{3+} in $CaWO_4:Eu^{3+}$ and Dy^{3+} in $CaWO_4:Ey^{3+}$ have been optimized to be 5 mol% and 3 mol% to Ca^{2+} in the phosphors for the achieving the highest PL intensities.

References

[1] Q. L. Dai, H. W. Song, X. Bai, G. H. Pan, S. Z. Lu, T. Wang, X. G. Ren, H. F. Zhao, J. Phys. Chem. C **111**, 7586 (2007).
[2] T. Qi, K. Takagi, J. Fukazawa, Appl. Phys. Lett. **36**, 278 (1980).
[3] S. Driscoll, U. S. Ozkan, Stud. Surf. Sci. Catal. **82**, 367 (1994).

[4] H. Wang, F. Medina, Y. Zhou, Q. Zhang Phys. Rev. B **45**, 10356 (1992).

[5] E. Ehrenbery, H. Weitzel, C. Heid, H. Fuess, G. Wltschek, T. Kroener, J. van Tol M. Bonnet, J. Phys-Condens. Matter. **9**, 3189 (1997).

[6] H. Meyssamy, K. Riwotzki, Adv. Mater. **11**, 840 (1999).

[7] M. Yada, M. Mihara, S. Mouri, S. Kijima Adv. Mater. **14**, 309 (2002).

[8] R. Meltzer, S. Feofilov, B. Tissue, Phys. Rev. B **60**, 14012 (1999).

[9] J. Shin, G. Hoven, A. Polman, Appl. Phys. Lett. **66**, 2379 (1995).

[10] M. Fu, M. Yoshida, Y. Kanzawa, S. Hayashi, K. Yamamoto, Appl. Phys. Lett. **77**, 1198 (1997).

[11] M. Nikl, P. Bohacek, E. Mihokova, E. Kobayashi, M. Ishii, Y. Usuki, V. Babin, A. Stolovich, S. Zazubovich, M. Bacci J. Lumin. **87**, 1136 (2000).

[12] E. F. Paski, M. W. BladesAnal. Chem. **60**, 1224 (1988).

[13] G. Blasse, L. H. Brixner, Chem. Phys. Lett. **173**, 409 (1990).

[14] Z. D. Lou, M. Cocivera Mater. Res. Bull. **37**, 1573 (2002).

[15] F. Wen, X. Zhao, H. Huo, J. Chen, E. Lin, J. Zhang Mater. Lett. **55**, 152 (2002).

[16] H. Deng, X. Li, Q. Peng, X. Wang, J. Chen, Y. Li, Angew. Chem. Int. Ed. **44**, 2782 (2005).

[17] Z. L. Wang, X. J. Feng, Phys. Chem. B **107**, 13563 (2003).

[18] C. X. Li, Z. W. Quan, J. Yang, P. P. Yang, J. Lin, Inorg. Chem. **46**, 6329 (2007).

[19] S. Murakami, H. Markus, R. Doris, M. Makato, Inorg. Chim. Acta. **300**, 1014 (2000).

[*]Corresponding author: piaoping@ciac.jl.cn